Quantum Electronics **51** (12) 1068–1075 (2021)

https://doi.org/10.1070/QEL17664

Mid-IR supercontinuum generation initiated by two-cascade stimulated Raman scattering in D_2-filled revolver fibre

Yu.P. Yatsenko, A.V. Gladyshev, I.A. Bufetov

Abstract. **We report a numerical study of coherent mid-IR supercontinuum generation at wavelengths above 2.4 μm, initiated by two-cascade stimulated Raman scattering in a deuterium-filled revolver fibre pumped by positively chirped picosecond pulses at a wavelength of 1.03 μm. It is shown that the highest efficiency of conversion to the second Stokes is ensured by fibre lengths at which the spectrum is strongly broadened by Kerr nonlinear effects. A range of optimal parameters (deuterium pressure, fibre length, pulse energy, and pulse duration) is found that ensure quantum efficiency at a level of 50% and a mid-IR supercontinuum width above 1000 nm. The coherence properties of the supercontinuum are shown to be determined by the pulse duration, the magnitude of the pulse chirp, and dispersion characteristics in each transmission band of the fibre. We demonstrate the feasibility of generating a single compressed mid-IR pulse of 20-fs duration with an energy of 1.9 μJ.**

Keywords: *hollow-core fibre, chirped picosecond pulses, stimulated Raman scattering, supercontinuum.*

1. Introduction

Owing to its unique power, guidance, and dispersion characteristics, gas-filled hollow-core fibre (HCF) with a microstructured silica cladding is widely used to convert spectral and temporal characteristics of light that are due to nonlinear effects in various gases [1–4]. Using a hydrogen-filled kagomé cladding HCF, Belli et al. [5] obtained a supercontinuum spanning the spectral range from the vacuum UV (124 nm) to the near-IR (1200 nm) under pumping at a wavelength λ = 805 nm by 30-fs microjoule pulses. According to their theoretical estimates [5], the supercontinuum was initiated by Kerr nonlinearity, as in previous studies [2, 3]. The effect of transient stimulated Raman scattering (SRS) showed up in the soliton compression step, where trailing edge self-steepening and pulse envelope breakdown led to impulsive excitation of coherent molecular vibrations.

The advent of revolver-type antiresonant HCF, with a cladding in the form of a single ring of cylindrical capillaries, first demonstrated by Pryamikov et al. [6], opened up new possibilities for mid-IR supercontinuum generation owing to the use of the multiband structure of such fibre [7–9]. Cassataro et al. [10] used krypton-filled single-ring photonic crystal fibre, having one, broad transmission band with one dispersion zero, for coherent supercontinuum generation between 300 nm and 3.1 μm under pumping with transform-limited 28.5-fs pulses at λ = 1.7 μm from a parametric generator. Yatsenko et al. [11] demonstrated supercontinuum generation in the spectral range 415–1593 nm, spanning 11 transmission bands of an atmospheric air-filled revolver HCF, under pumping with transform-limited 205-fs pulses at λ = 1.03 μm. According to numerical analysis results, dispersive waves and cascade nonlinear four-wave processes near dispersion zeros play a key role in energy transfer from one band to another and the supercontinuum can be extended well into the mid-IR, up to 4200 nm. A krypton-filled HCF with triangular capillaries was used for coherent supercontinuum generation in the range 0.2–1.7 μm, spanning several transmission bands, under pumping with 80-fs pulses at λ = 800 nm [12]. A high degree of coherence was ensured by the generation of dispersive waves on both sides of the resonance during accelerated high-order soliton decay upon a nonadiabatic dispersion growth on transmission band boundaries.

Along with studies in which a defining role in supercontinuum generation by femtosecond pulses is played by nonlinear effects, such as self-phase modulation (SPM), cross-phase modulation (XPM), and four-wave mixing (FWM), considerable research effort has been concentrated on the use of SRS as a main nonlinear process for broadband generation in the wavelength range corresponding to rotational and vibrational levels of molecular gases [13–18]. SRS in molecular gases with large frequency shifts of vibrational levels (4155 cm^{-1} in hydrogen and 2987 cm^{-1} in deuterium) allows for conversion of broadband femtosecond pulses from the near- to mid-IR in a single- and a two-cascade process. However, in going to very short pulses, much shorter than the dephasing time of an active gas, the SRS process becomes less steady, and the effect of SPM increases, considerably reducing conversion efficiency [16]. This limitation can be overcome by prechirping femtosecond pulses, which increases their duration [13].

Important properties of the SRS conversion of chirped pulses are coherence and that the sign and magnitude of the pump chirp remain unchanged in Stokes signals [15]. If only SRS is used for spectrum conversion, this allows for compression of chirped Stokes pulses in a compressor to the minimum possible level: the transform-limited pump pulse duration [18]. The combined effect of SRS, nonlinearity, and dispersion makes it possible to broaden the spectrum of chirped pulses in the Stokes region and simultaneously compress

Yu.P. Yatsenko, A.V. Gladyshev, I.A. Bufetov Prokhorov General Physics Institute of the Russian Academy of Sciences, Dianov Fiber Optics Research Center, ul. Vavilova 38, 119991 Moscow, Russia; e-mail: yuriya@fo.gpi.ru, alexglad@fo.gpi.ru, iabuf@fo.gpi.ru

Received 30 September 2021
Kvantovaya Elektronika **51** (12) 1068–1075 (2021)
Translated by O.M. Tsarev

them right in the fibre to durations shorter than the input pump pulse duration [19, 20].

The single-ring hollow-core silica fibre design makes it possible to obtain a broad transmission band with low losses in the mid-IR spectral region (2.4–5 μm) and flexibly tune transmission bands in other visible and near-IR ranges to pump wavelengths and cascade Stokes shifts in an active gaseous medium. In a recent study by Gladyshev et al. [21], chirped picosecond pulses were efficiently converted from the near- to mid-IR in a 1.03 → 1.49 → 2.68 μm two-cascade SRS process using three transmission bands of deuterium-filled HCF. That work demonstrated for the first time generation of femtosecond pulses in silica fibre at mid-IR wavelengths exceeding the long-wavelength edge of the 2.4-μm transmission band of silica. The energy of 920-fs pulses at a wavelength of 2.68 μm was 10 μJ, which was at least two orders of magnitude higher than previously reported energies of subpicosecond mid-IR pulses. The quantum efficiency of conversion to the second Stokes was 28%. All results in that study [21] were obtained at one deuterium pressure (5 atm) and one fibre length (2.9 m). Moreover, in that study SRS always prevailed over Kerr nonlinearity. For this reason, mid-IR supercontinuum generation conditions were not identified.

In this paper, we present a numerical analysis of a 1.03 → 1.49 → 2.68 μm two-cascade SRS process in deuterium-filled HCF at the fibre parameters and pulse energies used in previous work [21], in wide ranges of chirped pulse durations, deuterium pressures, and fibre lengths. We have demonstrated that conversion to the second Stokes has the highest efficiency at fibre lengths at which the spectrum is strongly broadened by Kerr nonlinear effects. We have found the region of optimal parameters (deuterium pressure, fibre length, pulse energy, and pulse duration) that ensure quantum efficiency at a level of 50% and a mid-IR supercontinuum width above 1000 nm. Coherence properties of the supercontinuum have been shown to be determined in considerable measure by the pulse duration and chirp, as well as by dispersion characteristics in each transmission band of the fibre. We have demonstrated the possibility of generating a single compressed mid-IR pulse of 20-fs duration with an energy of 1.9 μJ.

2. Numerical analysis method

In numerical analysis of SRS conversion in revolver fibre, we used a generalised nonlinear Schrödinger equation for the complex-valued spectral pulse envelope $\tilde{A}(z,\omega)$ [22], which takes into account higher order dispersion, Kerr nonlinearity, and SRS by Q2 vibrations of a deuterium molecule:

$$\frac{\mathrm{d}[\tilde{A}(z,\omega)\exp(-\hat{L}(\omega)z)]}{\mathrm{d}z} = \mathrm{i}\bar{\gamma}(\omega)\exp(-\mathrm{i}\hat{L}(\omega)z)$$

$$\times F\left\{\bar{A}(z,T)\int_{-\infty}^{\infty}R(T')\,|\bar{A}(z,T-T')|^2dT'\right\}, \qquad (1)$$

where

$$\bar{A}(z,T) = F^{-1}\left\{\frac{\tilde{A}(z,\omega)}{A_{\mathrm{eff}}^{1/4}(\omega)}\right\};$$

$$\bar{\gamma}(\omega) = \frac{N_2 n_0 \omega}{c n_{\mathrm{eff}}(\omega) A_{\mathrm{eff}}^{1/4}(\omega)}$$

is a nonlinear response;

$$\hat{L}(\omega) = i[\beta(\omega) - \beta(\omega_0) - \beta_1(\omega_0)(\omega - \omega_0)] - \frac{\alpha(\omega)}{2}$$

is a linear dispersion operator; $T = t - \beta_1 z$ is the time in a frame moving at the group velocity of the pulse envelope; $n_{\mathrm{eff}}(\omega)$ and $A_{\mathrm{eff}}(\omega)$ are the frequency-dependent effective refractive index and effective mode area; $\beta(\omega_0)$ and $\beta_1(\omega_0)$ are the propagation constant and its first derivative at the centre frequency of pump pulses; $\alpha(\omega)$ is the waveguiding loss; n_0 and N_2 are the linear and nonlinear refractive indices; c is the speed of light; and F and F^{-1} denote the forward and inverse Fourier transformations.

The nonlinear response function of deuterium has the form $R(t) = (1 - f_{\mathrm{R}})\delta(t) + f_{\mathrm{R}}h_{\mathrm{R}}(t)$. Here, the former term, with the delta function, represents the Kerr effect and the latter term represents the contribution of the SRS response, which relaxes more slowly. The SRS response function of deuterium, $h_{\mathrm{R}}(t)$, was represented by a relation for a damped oscillator: $h_{\mathrm{R}}(t) = \Omega^2\tau_{\mathrm{s}}\exp(-t/\tau_{\mathrm{d}})\sin(t/\tau_{\mathrm{s}})$, where $\Omega^2 = \tau_{\mathrm{s}}^{-2} + \tau_{\mathrm{d}}^{-2}$; $\tau_{\mathrm{s}} = 1/\omega_{\mathrm{R}}$; $\omega_{\mathrm{R}} = 5.626 \times 10^{14}$ s^{-1} is the cyclic frequency of molecular vibrations; $\tau_{\mathrm{d}} = T_2/2\pi$; and T_2 is the transverse dipole relaxation time of an excited-state vibrational level. In determining $T_2 = 1/(\pi\Delta\nu_{\mathrm{R}})$, we took into account the dependence of the linewidth $\Delta\nu_{\mathrm{R}}$ on the density ρ of the gas in the form $\Delta\nu_{\mathrm{R}} = 101/\rho + 120\rho$, where $\Delta\nu_{\mathrm{R}}$ (FWHM) is measured in megahertz, and ρ, in amagats [23]. The nonlinear refractive index N_2 was determined from data reported by Wahlstrand et al. [24]: at a deuterium pressure of 1 atm in the femtosecond range, they separately measured the contributions of electron Kerr nonlinearity ($N_{2\mathrm{K}} = 5.8 \times 10^{-24}$ m^2 W^{-1}) and the vibrational ($N_{2\mathrm{vib}} = 1.2 \times 10^{-24}$ m^2 W^{-1}) and rotational ($N_{2\mathrm{rot}} = 3.9 \times 10^{-24}$ m^2 W^{-1}) components of Raman scattering to the nonlinear refractive index. In numerical simulation, the contribution of the rotational component was left out of account because there was no experimental evidence of rotational SRS in previous work [21]. $N_{2\mathrm{K}}$ was taken to be a linear function of pressure p. $N_{2\mathrm{vib}}$ as a function of p was determined with allowance for the pressure dependence of the Raman transition linewidth $\Delta\nu_{\mathrm{R}}$ and upper-level population, which appear in the relation for the steady-state SRS gain coefficient $g(\Omega)$ [23]. The coefficient f_{R}, characterising the SRS contribution to the nonlinear refractive index, was evaluated as [25]

$$f_{\mathrm{R}}(p) = \frac{N_{2\mathrm{vib}}(p)}{N_2(0,p)} = \frac{4\int_0^{\infty}F^{-1}[\mathrm{Im}(N_{2\mathrm{vib}}(\Omega,p))\,\mathrm{d}t]}{N_2(0,p)},$$

where F^{-1} is the inverse Fourier transformation of the imaginary part of the nonlinear refractive index, related to the gain coefficient by $\mathrm{Im}(N_{2\mathrm{vib}}(\Omega,p)) = \lambda_0 g(\Omega,p)/4\pi$, and $N_2(0,p) = N_{2\mathrm{K}}p + N_{2\mathrm{vib}}(p)$.

Numerical analysis was carried out in the Matlab environment using built-in algorithms for performing the fast Fourier transform and solving the equation by the fourth-order Runge–Kutta method for the fundamental mode of the fibre, with allowance for the spectral dependences of the effective mode area $A_{\mathrm{eff}}(\omega)$, waveguiding loss $\alpha(\omega)$, and effective refractive index $n_{\mathrm{eff}}(\omega)$. The spectral range containing the first four transmission bands was divided into 2^{16} intervals. The maximum time interval was then 120 ps, and the minimum grid size was 1.8 fs. The main calculation results were obtained for positively chirped Gaussian input pulses with an amplitude

$$A = \sqrt{P}\exp\left(-\frac{1+\mathrm{i}C}{2}\frac{T^2}{T_0^2}\right).$$

Their power P, full width at half maximum ($\tau_{\mathrm{FWHM}} = 1.665T_0$), and chirp C corresponded to the output characteristics of the femtosecond laser (TETA-6, Avesta) used in previous work [21]. Transform-limited 250-fs pulses at a wavelength of 1.03 μm could be stretched through a negative chirp to 10 ps (chirp $C = 40$), with an energy of the order of hundreds of microjoules.

At each given energy, pulse duration, and gas pressure, we optimised the fibre length so as to maximise the efficiency of conversion to the second Stokes (with respect to the input pulse energy at a pump wavelength of 1.03 μm) for the 1.03 → 1.49 → 2.68 μm two-cascade SRS process.

3. Dispersion and guidance properties of the revolver HCF

The parameters of the ten-capillary revolver HCF, with a core diameter of 75 μm and capillary wall thickness of 1.15 μm, corresponds to the HCF used in previous work [21]. Its guidance and dispersion characteristics were calculated by the finite element method using standard COMSOL software. Figure 1a shows the theoretically calculated fundamental-mode loss in the spectral range corresponding to the first four transmission bands. The pump (1.03 μm), first Stokes (1.49 μm), and second Stokes (2.68 μm) wavelengths lie in the minimum loss region: in the third, second, and first bands of the fibre, respectively. At the same time, the first anti-Stokes wavelength (788 nm) lies in the peak loss region, which considerably impairs the efficiency of energy transfer to the anti-Stokes region through coherent four-photon processes.

Dispersion properties of the fibre were calculated with allowance for waveguiding dispersion and the dispersion of deuterium [26]. Figures 1b–1d show the variation of the fundamental-mode group velocity dispersion in the pump, first Stokes, and second Stokes wavelength ranges as the deuterium pressure is raised from 0 to 50 atm in 10-atm steps. In this pressure range, the dispersion at the pump wavelength can change its sign, whereas it is always negative at the first-Stokes wavelength and always positive at the second-Stokes wavelength (vertical dashed lines in Figs 1b–1d). At a pressure of 50 atm, the dispersion at the pump, first Stokes, and second Stokes wavelengths is 0.17, −0.2, and 4.6 ps^2 km^{-1}, respectively.

4. Numerical simulation results and discussion

Figure 2 shows the maximum SRS (1.03 → 2.68 μm) quantum efficiency (QE) and the corresponding optimal fibre length L_{opt} as functions of pulse energy at deuterium pressures of 5 and 50 atm.

At a pressure of 5 atm, QE rises monotonically from 0.13 to 0.36 as the pulse energy increases from 50 to 300 μJ, which is accompanied by a decrease in L_{opt} from 11 to 1 m. It is worth noting good agreement between the QE (0.25) obtained numerically at a pulse energy of 100 μJ ($L_{\mathrm{opt}} = 3.1$ m) and the value obtained experimentally (0.24) under similar conditions in previous work [21].

At a pressure of 50 atm, QE is considerably higher, with a maximum (51%) at a pulse energy in the range 50–60 μJ and $L_{\mathrm{opt}} \sim 2.5$–$2.7$ m (Fig. 2a). Moreover, over the entire range of

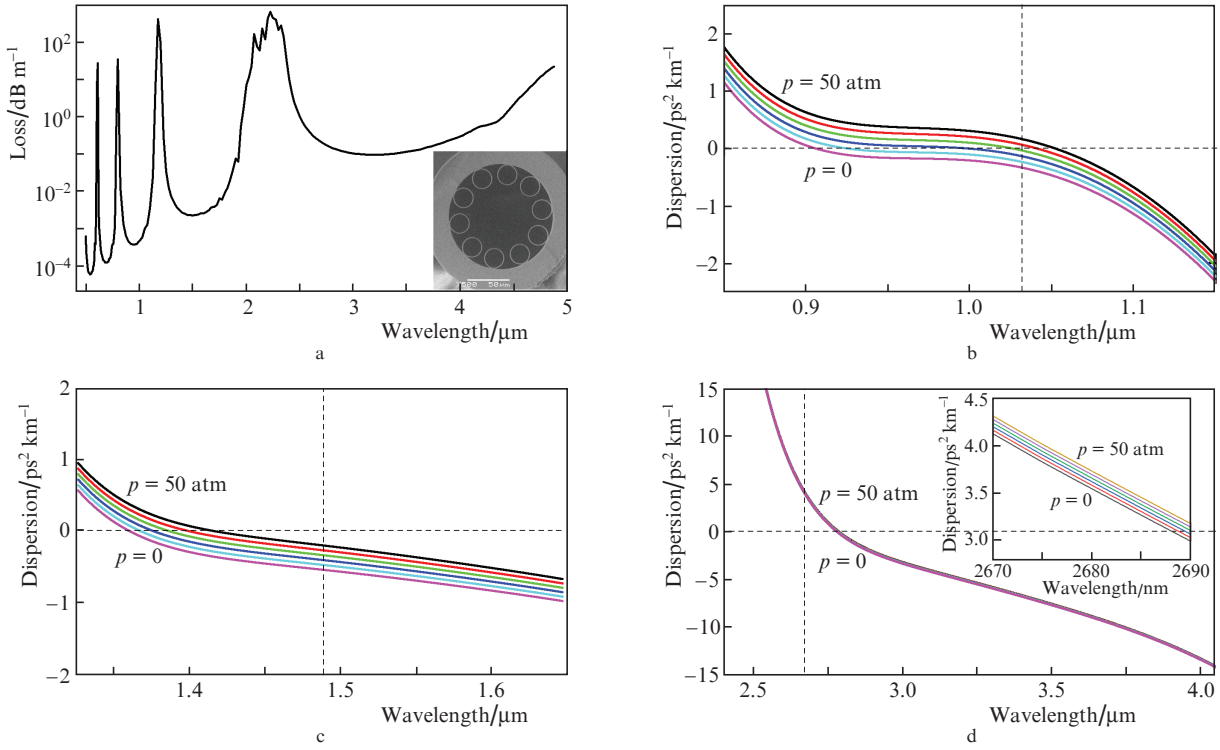

Figure 1. (Colour online) Fundamental-mode waveguiding loss in the hollow-core fibre in the range 0.6–5 μm (a) (inset: cross-sectional electron micrograph of the fibre) and calculated fundamental-mode dispersion as a function of wavelength at various deuterium pressures ($p = 0$–50 atm) for the first (b), second (c), and third (d) transmission bands [inset in panel d: enlarged portion around the second-Stokes wavelength (2.68 μm)].

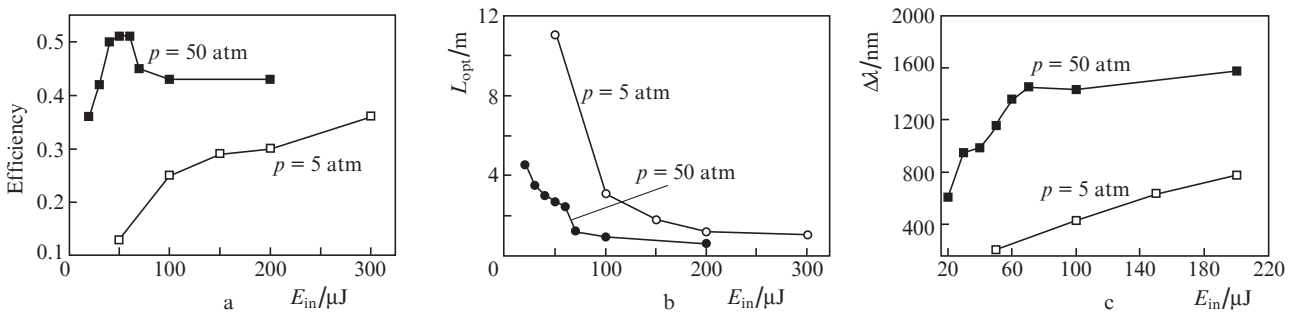

Figure 2. (a) Maximum 1.03 → 2.68 μm SRS conversion quantum efficiency, (b) optimal fibre length, and (c) spectral width of the supercontinuum at mid-IR wavelengths above 2.4 μm as functions of input pulse energy at deuterium pressures of 5 and 50 atm. Input pulse duration, 10 ps; chirp $C = 40$.

pulse energies examined, QE is higher and L_{opt} is smaller than those at a pressure of 5 atm. The distinction can be accounted for by the increase in the concentration of active molecules and the appreciable decrease in the transverse relaxation time of the T_2 excited-state vibrational level – from 480 ps at a pressure of 5 atm to 49 ps at 50 atm – which makes the SRS process less unsteady, thus improving conversion efficiency at high pressures.

Figure 3 demonstrates how the pump, first Stokes, and second Stokes spectra vary along the fibre length (L) at an input pulse energy of 50 μJ, pulse duration of 10 ps (chirp $C = 40$), and pressures of 5 and 50 atm. The transformation of the spectra in the initial part of the fibre is determined by the SRS process and is characterised by a narrow spectrum at Stokes wavelengths. The subsequent broadening of the spectrum due to nonlinear processes leads to a strong modulation of the spectrum even over the first metres of the fibre. It can be seen that, at a pressure of 50 atm, the pump and Stokes signal spectra are considerably broader, because Kerr nonlinearity is an order of magnitude stronger. At a pressure of 50 atm and fibre length above 2 m, corresponding to the maximum QE of conversion to the second Stokes (51%), the spectrum at wavelengths above 2.4 μm has the form of a supercontinuum with a –20-dB width of 1100 nm (Figs 2c, 3b).

It follows from Figs 2 and 3 that, independent of deuterium pressure, the highest efficiency of conversion to the second Stokes is achieved at fibre lengths corresponding to considerable broadening of the spectrum. Therefore, the most efficient energy transfer to the mid-IR is ensured by the combined effect of SRS and nonlinear processes that broaden the spectrum, such as XPM, SPM, and FWM.

The effect of Kerr nonlinearity on the broadening of the spectrum increases with decreasing input chirped pulse duration at a constant pulse energy. Figures 4 and 5 show variations in spectra, the temporal structure, and QE along the fibre length at a pulse energy of 50 μJ, pulse duration of 1 ps ($C = 4$), and deuterium pressure of 50 atm. As at a pulse duration of 10 ps, here supercontinuum generation along the fibre length begins with SRS pump conversion to the first and second Stokes. However, the higher peak power of 1-ps input pulses leads to a stronger effect of Kerr nonlinear processes. Comparison with Fig. 3b indicates that, at a pulse duration of 1 ps, broadening of the spectrum begins at shorter fibre lengths (even at $L > 0.2$ m). At $L_{opt} = 1$ m, corresponding to the highest QE (0.22) of conversion to the second Stokes (Fig. 4b), the mid-IR supercontinuum has a broader spectrum, reaching 1788 nm. The time dependences shown in Fig. 5 are characterised by splitting of the pump pulse enve-

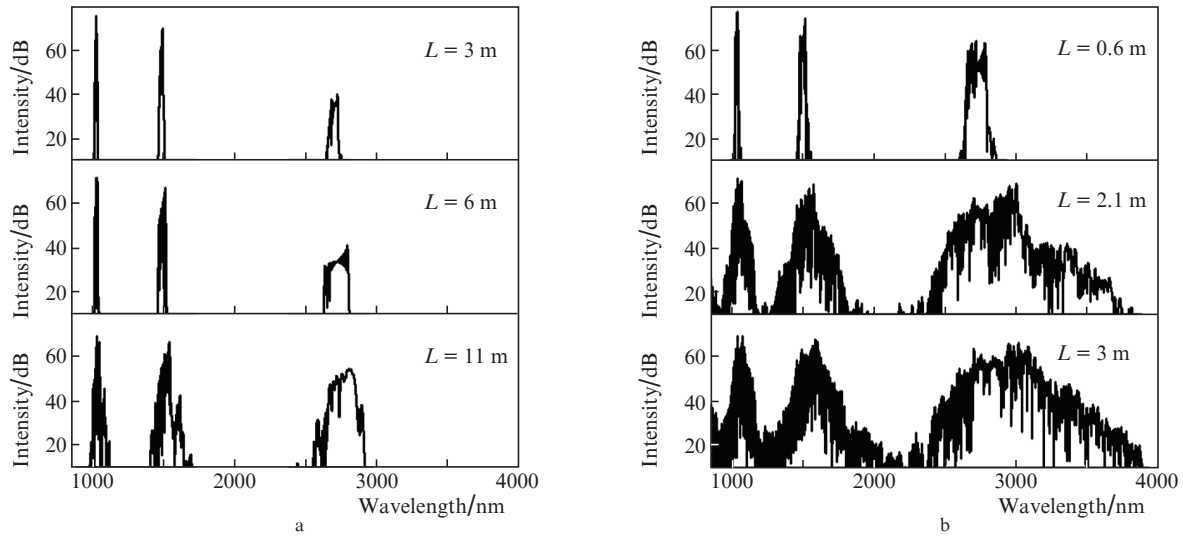

Figure 3. Variation of the pump, first Stokes, and second Stokes spectra along the fibre length (L) at an input pulse energy of 50 μJ, input pulse duration of 10 ps, chirp $C = 40$, and deuterium pressures of (a) 5 and (b) 50 atm.

lope and Stokes signals into sharp soliton-like peaks differing in amplitude and phase, whose number increases with increasing fibre length. In this context, there is particular interest in oscilloscope traces of the second Stokes at fibre lengths of 0.2 and 1 m, which demonstrate the formation of single compressed mid-IR femtosecond pulses. At $L = 0.2$ m, the pulse shape and the spectrum of the second Stokes remain relatively smooth (and have one main peak and one satellite). The duration of the main peak is 80 fs (compression ratio $\kappa = 12.5$), and the corresponding energy is 48% of the total second Stokes energy (1.15 μJ) at this fibre length. An even stronger compression was obtained at a fibre length of 1 m, corresponding to the highest QE (0.22) at an input pulse duration of 1 ps ($C = 4$). Here, the large shift of the spectrum to the negative dispersion region led to the formation of a single compressed ($\kappa = 50$) 20-fs pulse in the wavelength range of the second Stokes, with a pulse energy of 1.9 μJ, which amounted to 44% of the total energy in the mid-IR.

A more detailed analysis of the spectra and temporal structure of pump pulses and Stokes signals at small fibre lengths, 0.2–1 m (Fig. 5), makes it possible to assess the effect of dispersion characteristics in transmission bands on interac-

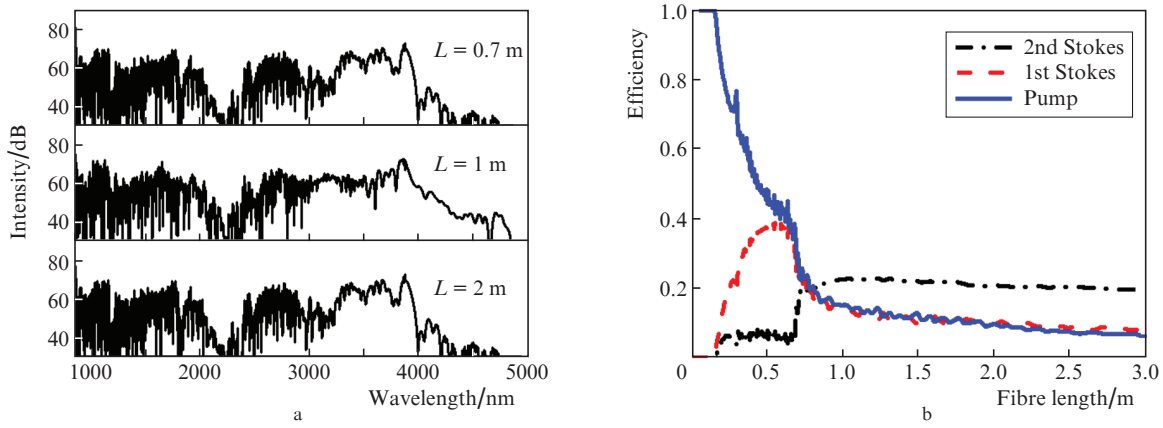

Figure 4. (Colour online) Variation of the (a) spectrum and (b) conversion quantum efficiency for the first and second Stokes along the fibre length at an input pulse energy of 50 μJ, input pulse duration of 1 ps, chirp $C = 4$, and deuterium pressure of 50 atm.

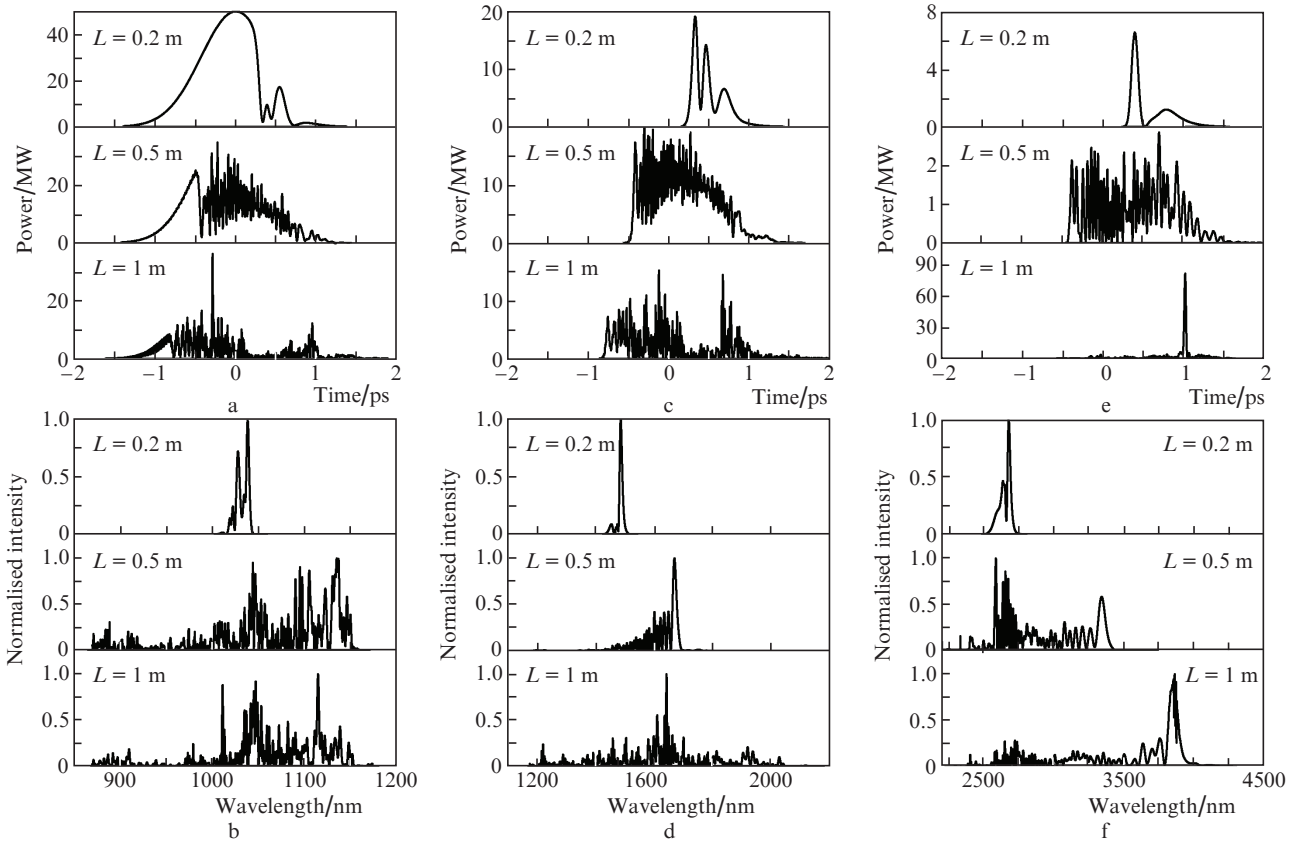

Figure 5. Variation of the temporal structure and spectrum of the (a, b) pump, (c, d) first Stokes, and (e, f) second Stokes along the fibre length at an input pulse energy of 50 μJ, deuterium pressure of 50 atm, input pulse duration of 1 ps, and chirp $C = 4$.

tion between SRS and other nonlinear processes. Up to a fibre length of 0.5 m, there is pump energy transfer to Stokes signals at the pump pulse trailing edge, characteristic of pure near-threshold SRS, where the pulse leading edge energy goes into excitation of resonance molecular vibrations. Further light propagation through the fibre is characterised by considerable broadening of the spectrum by XPM. An asymmetric modulation of the spectrum with a shift to longer wavelengths, characteristic of XPM, is observed around the first and second Stokes wavelengths (Figs 5d, 5f), and the effect of dispersion increases and shows up differently in these regions.

The pump-to-first Stokes energy conversion quantum efficiency reaches a maximum (38%) at a fibre length of 0.5 m (Fig. 4b). The increase in peak power is accompanied by distortion of the temporal profile of the first-Stokes pulse envelope due to modulation instability. The steepening of the pump pulse trailing edge, caused by the more active energy transfer to the Stokes regions at the trailing edge, leads to splitting of the pump pulse envelope and the formation of first-Stokes modulation pulses of duration $\tau_{FWHM} \sim 80$ fs at a fibre length of 0.2 m (Fig. 5c). In the case of chirped pulses of this duration, the dispersion length is considerably smaller: at $C = 4$, it is $L_d = \tau^2_{FWHM}/[(1.665)^2|\beta_2|(1 + C^2)] = 0.68$ m. The nonlinear length for interaction of Stokes pulses with pump light through XPM is $L_{nl} = 1/(2\gamma_{1S}P_p) = 0.02$ m at $P_p = 50$ MW ($\gamma_{1S} = \lambda_p A_{eff\,p}\gamma_p/(\lambda_{1S}A_{eff\,1S}) \approx 5 \times 10^{-7}$ m^{-1} W^{-1}, $\gamma_p = 2\pi N_{2K} \times (\lambda_p A_{effp})^{-1}$, $N_{2K} = 1.95 \times 10^{-22}$ m^2 W^{-1}, $A_{eff\,p} \approx A_{eff\,1S} = 2460$ m^2, $\lambda_p = 1.03$ μm, and $\lambda_{1S} = 1.49$ μm). Thus, the first-Stokes modulation pulse at a fibre length of 0.2 m has a soliton order $N = \sqrt{L_d/L_{nl}} = 5.8$, and soliton fission under the effect of higher order dispersion terms and self-steepening, which are coherent effects, may occur at a fibre length $L_{fiss} = L_D/N = 0.12$ m. Modulation instability development from spontaneous noise occurs over a length [27] $L_{sp} \approx 16N_{nl} = 0.32$ m, which is consistent with the development of chaotic modulation of the pulse envelope at fibre lengths from 0.3 to 0.5 m (Figs 5a, 5c, 5e). Since L_{fiss} is comparable to L_{sp}, Stokes generation at first-Stokes wavelengths is strongly influenced by four-wave processes, which amplify spontaneous noise and impair light coherence.

The modulation structure of the pulse envelope and second-Stokes spectrum is formed under the effect of modulation structures of first-Stokes pulses (via SRS) and pump pulses (via XPM). The process occurs at a large difference in group velocity between the second and first Stokes ($d = 1/v_{2S} - 1/v_{1S} = 0.95$ ps m^{-1}) and between the second Stokes and pump ($d = 1/v_{2S} - 1/v_p = 0.89$ ps m^{-1}). At a fibre length of 0.2 m, where the main modulation pulse duration is ~80 fs, like the first-Stokes pulse duration, the pulse mismatch length is $L_w = \tau_{FWHM}/1.665/d = 0.05$ m, which leads to deeper modulation of the second-Stokes pulse structure at small fibre lengths and a longer amplification phase. The highest QE (0.22) is reached at fibre lengths of ~1 m, where the temporal structure of pump pulses and Stokes signals completely loses its constant component and consists of separate femtosecond pulses.

At a small fibre length (under 0.2 m), second-Stokes amplification occurs in the positive dispersion region of the first transmission band of the fibre (zero dispersion wavelength $\lambda_{02S} = 2.77$ μm), but even at fibre lengths exceeding 0.3 m the asymmetric shift of the first-Stokes spectrum leads to an asymmetric shift of the second Stokes spectrum to the long-wavelength negative dispersion region. A second-Stokes pulse of 80-fs duration (with allowance for the effect of pump XPM and under the condition that the chirp remains $C = 4$) has a soliton parameter $N = 0.9$ ($L_{nl} = 0.03$ m and $L_d = 0.04$ m). The smaller N in comparison with the one given above for the first Stokes is ensured by the two orders of magnitude higher group velocity dispersion at the second-Stokes wavelength (2.68 μm), which facilitates single pulse isolation and compression during the supercontinuum formation process. Also important is that the first transmission band of the HCF, where second-Stokes modulation pulses propagate, has only one resonance absorption peak and is characterised by a large slope of the dispersion curve (Fig. 1d). This increases the effect of higher order dispersion terms on soliton fission. At a wavelength of 3.2 μm, corresponding to the maximum in the spectrum of a single 20-fs pulse, β_2 and β_3 are -5.1 ps^2 km^{-1} and -0.012 ps^3 km^{-1}, respectively, and the second- and third-order dispersion lengths are comparable ($L_d = \tau^2_{FWHM}/[(1.665)^2|\beta_2|] = 28.3$ μm and $L'_d = \tau^3_{FWHM}/[(1.665)^2|\beta_3|] = 144.4$ μm). Owing to the large frequency detuning and small spectral width of vibrational levels in gases, there is no SRS-induced soliton self-shift, so the third- and higher order dispersion is the main effect responsible for the formation of a single pulse on account of the larger shift of a soliton with the largest amplitude to longer wavelengths.

It follows from Fig. 5f that the spectrum of a single 20-fs compressed pulse formed over a fibre length of 1 m shifted to the wavelength range 2.9–3.7 μm, improving supercontinuum coherence in this part of the mid-IR (Fig. 6). However, modulation instability development from spontaneous noise occurs at a fibre length as short as $L_{sp} = 0.48$ m, and its effect seems to be responsible for the fact that the compressed pulse energy is just 44% of the total supercontinuum energy at wavelengths above 2.4 μm. Besides, because of the modulation instability, the compressed pulse propagation length in the fibre does not exceed 10–15 cm.

The feasibility of isolating and compressing a single pulse is determined by the degree of supercontinuum coherence. To evaluate it, we used the first-order correlation function $|g^{(1)}(\lambda)|$ [27]. The average over an ensemble of 200 independent pairs of spectral amplitudes was determined from 20 separate two-cascade SRS realisations with allowance for random phase noise. Like Dudley and Coen [28], as the main noise process influencing modulation instability we used quantum noise, which was introduced additively to the input pulse amplitude, with an amplitude corresponding to one photon in the frequency range under study and a random phase.

Figure 6 illustrates how coherence properties of supercontinuum vary along the fibre length for 10-ps (chirp $C = 40$) and 1-ps ($C = 4$) pulses at an input energy of 50 μJ in both cases and a deuterium pressure of 50 atm. A high degree of coherence throughout the spectral range studied was obtained at a fibre length of 0.2 m for both pulse durations (Figs 6a, 6d). Here the transformation of the spectrum is mainly due to a transient SRS process ($\tau < T_2$) characterised by a high degree of coherence [29]. At a fibre length of 1 m and pulse duration of 10 ps or a fibre length of 0.5 m and pulse duration of 1 ps, corresponding to the highest first-Stokes QE, the spectrum is already strongly broadened by nonlinear processes and the temporal envelope is modulated by numerous narrow peaks. A high degree of coherence persists in separate portions of the spectrum, in each transmission band (Figs 6b, 6e). The degree of coherence for a 10-ps pulse is here noticeably lower than that for a 1-ps pulse. At a fibre length of 3 m, corresponding to the highest QE of conversion to the second

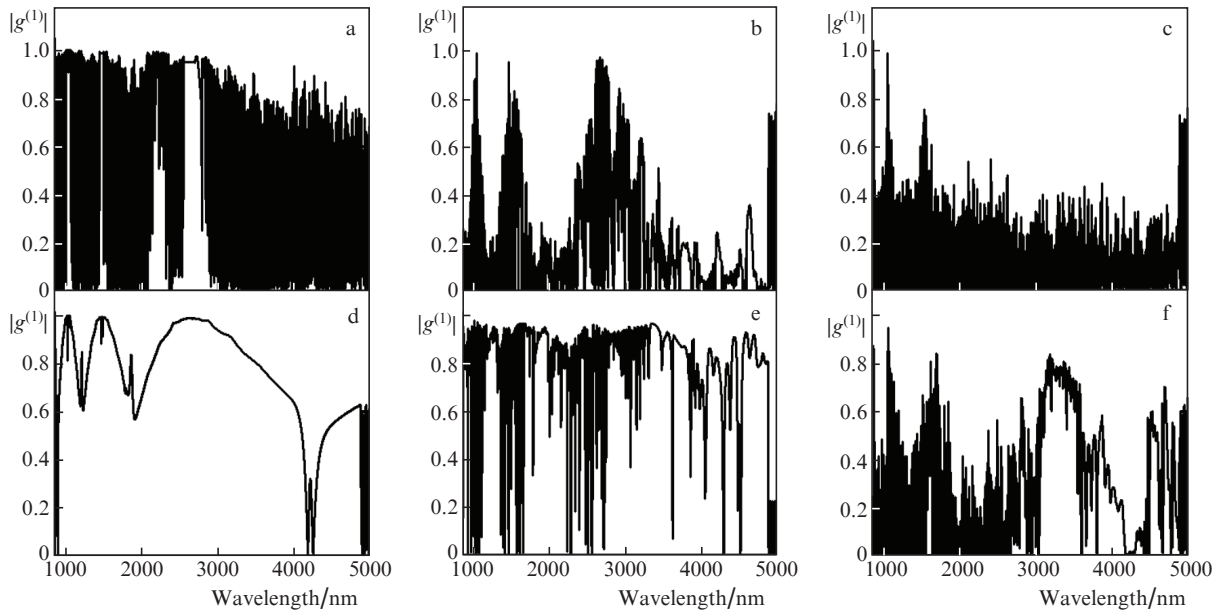

Figure 6. Degree of coherence of the spectrum as a function of wavelength for 10-ps pulses ($C = 40$) at a fibre length of (a) 0.2, (b) 1, and (c) 3 m and 1-ps pulses ($C = 4$) at a fibre length of (d) 0.2, (e) 0.5, and (f) 1 m. Input pulse energy, 50 μJ; deuterium pressure, 50 atm.

Stokes for a 10-ps pulse, mid-IR supercontinuum has low coherence (Fig. 6c). The lower coherence at the highest QE of conversion to the second Stokes for a 10-ps pulse in comparison with a 1-ps pulse can be accounted for by the fact that, at a given energy of 50 μJ, because the peak pump power is an order of magnitude lower, nonlinear processes have no time to produce a modulation structure consisting of separate soliton-like pulses over a fibre length of ~3 m. The small random modulation structure of the pump and Stokes signals had a constant component.

For a 1-ps pulse at the highest QE over a fibre length of 1 m, a relatively high degree of coherence ($|g^{(1)}(\lambda)| > 0.7$) was obtained in the wavelength range of the second Stokes (2900–3700 nm). Near the pump and first-Stokes wavelengths, we observe considerably narrower regions with a high degree of coherence (Fig. 6f). The higher degree of coherence in the wavelength range of the second Stokes is due to the formation of a single 20-fs pulse, whereas the temporal picture at the pump and first-Stokes wavelengths comprises numerous narrow modulation pulses (Fig. 5).

5. Conclusions

We have numerically demonstrated for the first time the feasibility of efficient coherent mid-IR supercontinuum generation at wavelengths above 2.4 μm as a result of the combined effect of cascade SRS and nonlinear processes in a gas-filled multiband revolver HCF pumped by positively chirped picosecond pulses at a wavelength of 1.03 μm. At chirped pulse durations from 1 to 10 ps (chirp $C = 4–40$) and pulse energies up to hundreds of microjoules, supercontinuum generation along the fibre length is initiated by SRS conversion of the spectrum in the first- and second-Stokes regions, located in different transmission bands of the fibre. Further pulse propagation through the fibre is accompanied by a strong influence of nonlinear effects, such as SPM, XPM, and FWM, which broaden the spectrum in the pump and Stokes regions. The highest QE can be reached in a range of parameters where the spectrum has the form of a multiband supercontinuum. The energy distribution over the spectrum and the degree of supercontinuum coherence depend on dispersion and guidance characteristics in each transmission band of the fibre and the chirped pulse duration.

For 10-ps pulses with a chirp $C = 40$ and, accordingly, the transform-limited spectral width of 250-fs pulses, at a deuterium pressure of 50 atm and pulse energy of 50 μJ, energy transfer to the second Stokes with QE over 50% is possible. The –20-dB spectral width at wavelengths above 2.4 μm is then 1100 nm. However, single pulse isolation in the mid-IR and a high degree of coherence of the broadened spectrum are here only possible in the initial stages of supercontinuum development, where the contribution of nonlinear processes is still small. With a decrease in chirped pulse duration and a proportional decrease in the magnitude of the chirp, the increasing impact of nonlinear effects leads to an increase in the width and degree of coherence of the mid-IR supercontinuum, but the efficiency of pump energy transfer to this region decreases. For chirped 1-ps pulses (chirp $C = 4$), we have demonstrated the feasibility of generating a single compressed mid-IR pulse of 20-fs duration with an energy of 1.9 μJ, which amounts to 44% of the total energy obtained at the highest QE in this range.

The present results suggest that cascade SRS in a gas-filled HCF with a broad transmission band in the range 3–5 μm in the mid-IR is potentially attractive for generating intense few-cycle femtosecond pulses during the supercontinuum formation process. Such pulses can be useful in optical coherence tomography [30] and many other biophotonic applications [31]. The above technique for generating such pulses allows one to use commercial femtosecond lasers of the micron range with transform-limited pulse durations more than one order of magnitude longer than the compressed pulse duration in the mid-IR. This can be an important advantage of this technique over alternative methods that employ more complex parametric oscillator designs for generating mid-IR femtosecond pulses.

Acknowledgements. This work was supported by the Russian Science Foundation (Project No. 19-12-00361).

References

1. Travers J.C., Chang W., Nold J., Joly N.Y., Russell P.St.J. *J. Opt. Soc. Am. B*, **28**, A11 (2011).
2. Joly N.Y., Nold J., Chang W., Hölzer P., Nazarkin A., Wong G.K.L., Biancalana F., Russel P.St.G. *Phys. Rev. Lett*., **106**, 203901 (2011).
3. Mak K.F., Travers J.C., Hölzer P., Joly N.Y., Russell P.St.J. *Opt. Express,* **21**, 10942 (2013).
4. Tani F., Travers J.C., Russell P.St.J. *J. Opt. Soc. Am. B*, **31**, 311 (2014).
5. Belli F., Abdolvand A., Chang W., Travers J.C., Russell P.St.J. *Optica,* **2**, 292 (2015).
6. Pryamikov A.D., Biriukov A.S., Kosolapov A.F., Plotnichenko V.G., Semjonov S.L., Dianov E.M. *Opt. Express*, **19**, 1441 (2011).
7. Bufetov I.A., Kosolapov A.F., Pryamikov A.D., Gladyshev A.F., Kolyadin A.N., Krylov A.A., Yatsenko Yu.P., Biriukov A.S. *Fibers*, **6**, 1 (2018).
8. Belardi W., Knight J.C. *Opt. Express*, **22**, 10091 (2014).
9. Poletti F. *Opt. Express*, **22**, 23807 (2014).
10. Cassataro M., Novoa D., Gunendi M.C., Edavalath N.N., Frosz M.H., Travers J.C., Russell P.St.J. *Opt. Express*, **25**, 7637 (2017).
11. Yatsenko Yu.P., Pletneva E.N., Okhrimchuk A.K., Gladyshev A.V., Kosolapov A.F., Kolyadin A.N., Bufetov I.A. *Quantum Electron*., **47**, 553 (2017) [*Kvantovaya Elektron*., **47**, 553 (2017)].
12. Sollapur R., Kartashov D., Zürch M., Hoffmann A., Grigorova T., Sauer G., Hartung A., Schwuchow A., Bierlich J., Kobelke J., Chemnitz M., Schmid M.A., Spielmann C. *Light: Sci. Appl*., **6**, e17124 (2017).
13. Jordan C., Stankov K.A., Marowsky G., Canto-Said E.J. *Appl. Phys. B*, **59**, 471 (1994).
14. Krylov V., Ollikainen O., Wild U.P., Rebane A., Bespalov V.G., Staselko D.I. *J. Opt. Soc. Am. B*, **15**, 2910 (1998).
15. Konyashchenko A.V., Losev L.L., Tenyakov S.Yu. *Opt. Express*, **15**, 11855 (2007).
16. Konyashchenko A.V., Kostryukov A.V., Losev L.L., Pazyuk V.S. *Quantum Electron*., **47**, 593 (2017) [*Kvantovaya Elektron*., **47**, 593 (2017)].
17. Vicario C., Shalaby M., Konyashchenko A., Losev L., Hauri C.P. *Opt. Lett*., **41**, 4719 (2016).
18. Didenko N.V., Konyashchenko A.V., Kostryukov A.V., Losev L.L., Pazyuk V.S., Tenyakov S.Yu., Molchanov V.Ya., Chizhikov S.I., Yushkov K.B. *Quantum Electron*., **45**, 1101 (2015) [*Kvantovaya Elektron*., **45**, 1101 (2015)].
19. Loranger S., Russell P.St.J., Novoa D. *J. Opt. Soc. Am. B*, **37**, 3550 (2020).
20. Gladyshev A.V., Astapovich M.S., Yatsenko Yu.P., Kosolapov A.F., Okhrimchuk A.K., Bufetov I.A. *Quantum Electron*., **49**, 1089 (2019) [*Kvantovaya Elektron*., **49**, 1089 (2019)].
21. Gladyshev A., Yatsenko Yu., Kolyadin A., Kompanets V., Bufetov I. *Opt. Mater. Express*, **10**, 3081 (2020).
22. Dudley J., Taylor R. *Supercontinuum Generation in Optical Fibers* (Cambridge: Cambridge University Press, 2010).
23. Ottush J.J., Rockwell D.A. *IEEE J. Quantum Electron*., **24**, 2076 (1988).
24. Wahlstrand J.K., Zahedpour S., Cheng Y.-H., Palastro J.P., Mildberg H.M. *Phys. Rev. A*, **92**, 063828 (2015).
25. Stolen R.H., Gordon J.P., Tomlinson W.J., Haus H.A. *J. Opt. Soc. Am. B*, **6**, 1159 (1989).
26. Larsén T. *Z. Phys.*, **100**, 543 (1936); https://doi.org/10.1007/BF01336710.
27. Dudley J.M., Genty G., Coen S. *Rev. Mod. Phys*., **78**, 1135 (2002).
28. Dudley J.M., Coen S. *Opt. Lett*., **27**, 1180 (2002).
29. Couny F., Carraz O., Benabid F. *J. Opt. Soc. Am. B*, **26**, 1209 (2009).
30. Su R., Kirillin M., Chang E.W., Sergeeva E., Yun S.H., Mattsson L. *Opt. Express*, **22**, 1584 (2014).
31. Tu H., Boppart S.A. *Laser Photonics Rev*., **7**, 628 (2013).